Fabrication of a Label-Free Electrochemical Immunosensor of Low-Density Lipoprotein

Wei Yan, Xiaojun Chen, Xinghua Li, Xiaomiao Feng, and Jun-Jie Zhu*

Key Laboratory of Analytical Chemistry for Life Science (MOE), School of Chemistry and Chemical Engineering, Nanjing University, Nanjing 210093, China

Received: August 15, 2007; In Final Form: November 9, 2007

The silver chloride@polyaniline (PANI) core−shell nanocomposites (AgCl@PANI) combined with Au nanoparticles (AuNPs) were used to prepare the AuNPs−AgCl@PANI hybrid material. A novel sensitive label-free low-density lipoprotein (LDL) electrochemical biosensor was fabricated by adsorption of antibody to apolipoprotein B-100 (aopB-100) on an AuNPs−AgCl@PANI-modified glassy carbon (GC) electrode. The hybrid material could provide surface for high antibody loading due to its large surface-to-volume ratio. Since each LDL has an apoB-100 on its phospholipids coat, they could be bonded to the electrode surface through the specific antibody−antigen reaction. Electrochemical impedance spectroscopy (EIS) was used to characterize the recognition of LDL. The negative charges carried by LDL phospholipids coat would block the electron transfer of the $[Fe(CN)_6]^{3-/4-}$ redox couple severely. In addition, the conductivity of LDL is very poor, so small amounts of LDL on the electrode could result in great change in the electron-transfer resistance (R_{et}). The biosensor exhibited a highly sensitive response to LDL with a detection limit of 0.34 pg/mL, and some factors that would affect the performance of the biosensor were studied, such as incubation time and temperature.

Introduction

Coronary heart disease (CHD) is one of the leading causes of mortality in not only the developed world but also in some developing countries.[1] Studies indicate that cholesterol-enriched low-density lipoprotein (LDL) in plasma can promote the deposition of plasma lipids in the artery wall and thereby elicit the formation of fatty streaks and/or atherosclerotic plaques.[2] CHD is the end result of the accumulation of atheromatous plaques within the walls of the arteries that supply the myocardium.[3] The structure of LDL contains, as depicted in Figure 1A, a hydrophobic core of about 1500 molecules of cholesteryl surrounded by a polar coat composed primarily of phospholipids and a 513 kDa protein called apolipoprotein B-100 (apoB-100).[4] ApoB-100 is synthesized by the liver and serves as a ligand for the LDL receptors on the surface of liver cells, which means LDL can be taken into a cell by endocytosis for degradation.[5] Mutations in either LDL receptor or apoB-100 will decrease the efficient receptor-mediated uptake of LDL and result in high level of LDL in plasma.[6,7]

The concentration of LDL-C (low-density lipoprotein cholesterol) has been used in clinic as one of the indicators for hyperlipidemia. Currently, the LDL-C concentration is estimated in most clinical laboratories by an indirect method that calculates the LDL cholesterol concentration according to Friedewald et al.[8] This approach derives the LDL-C from total cholesterol, HDL-C (high-density lipoprotein cholesterol), and VLDL-C (very low-density lipoprotein cholesterol) concentrations where the VLDL-C concentration is further estimated from the serum triglyceride concentration.[8,9] Recently, we have introduced a electrochemiluminescent way for the direct determination of the concentration of LDL,[10] and here a novel label-free biosensor with high sensitivity for the direct detection of the concentration LDL was constructed on the basis of the Au nanoparticle (AuNPs)−AgCl@polyaniline (PANI) hybrid material. The AuNPs−AgCl@PANI hybrid material was prepared by incorporation of AuNPs on the surface of AgCl@PANI core−shell nanocomposties.[11] The inorganic@conducting PANI nanocomposites have attracted significant academic and technological attention because of their unique properties as well as extensive applications in diverse areas.[12] Generally, acidic conditions (generally pH < 4) are required for the formation of the most highly conductive form of PANI,[13,14] and this greatly restricts its applications in bioelectrochemistry, which normally needs a neutral pH environment. However, AgCl@PANI nanocomposites had good redox activity at neutral aqueous solution,[11] and the incorporation of AuNPs has improved the electroactivity of AgCl@PANI further.

The hybrid material was cast on a glassy carbon (GC) electrode, and an electrochemical biosensor for the detection of LDL was constructed by adsorption of antibody to apoB-100 (anti-apoB-100) on the hybrid material, as shown in Figure 1B. The free active sites of the biosensor were saturated with BSA, and LDL could be bonded to the electrode surface through the specific immunoreaction between the apoB-100 on their phospholipids coats and anti-apoB-100 on the electrode surface. After that, the study on electrochemical impedance spectroscopy (EIS) was performed. The advantage of EIS over other electrochemical techniques is that only small-amplitude perturbations from steady state are needed, and information concerning the interface can be provided.[15] Several groups have utilized EIS to fabricate label-free high-sensitivity immuosensors.[15−20] Herein, the fabricated LDL immuosensor exhibited a highly sensitive response to LDL with a detection limit of 0.34 pg/mL. The high sensitivity could be ascribed to the large surface-to-volume ratio of AuNPs−AgCl@PANI, the poor conductivity of LDL, and the negative charges carried by its phospholipids coat.

* Corresponding author: tel 86-25-8359-4976; fax +86-25-8359-4976; e-mail jjzhu@nju.edu.cn.

10.1021/jp0765594 CCC: $40.75
Published on Web 01/09/2008

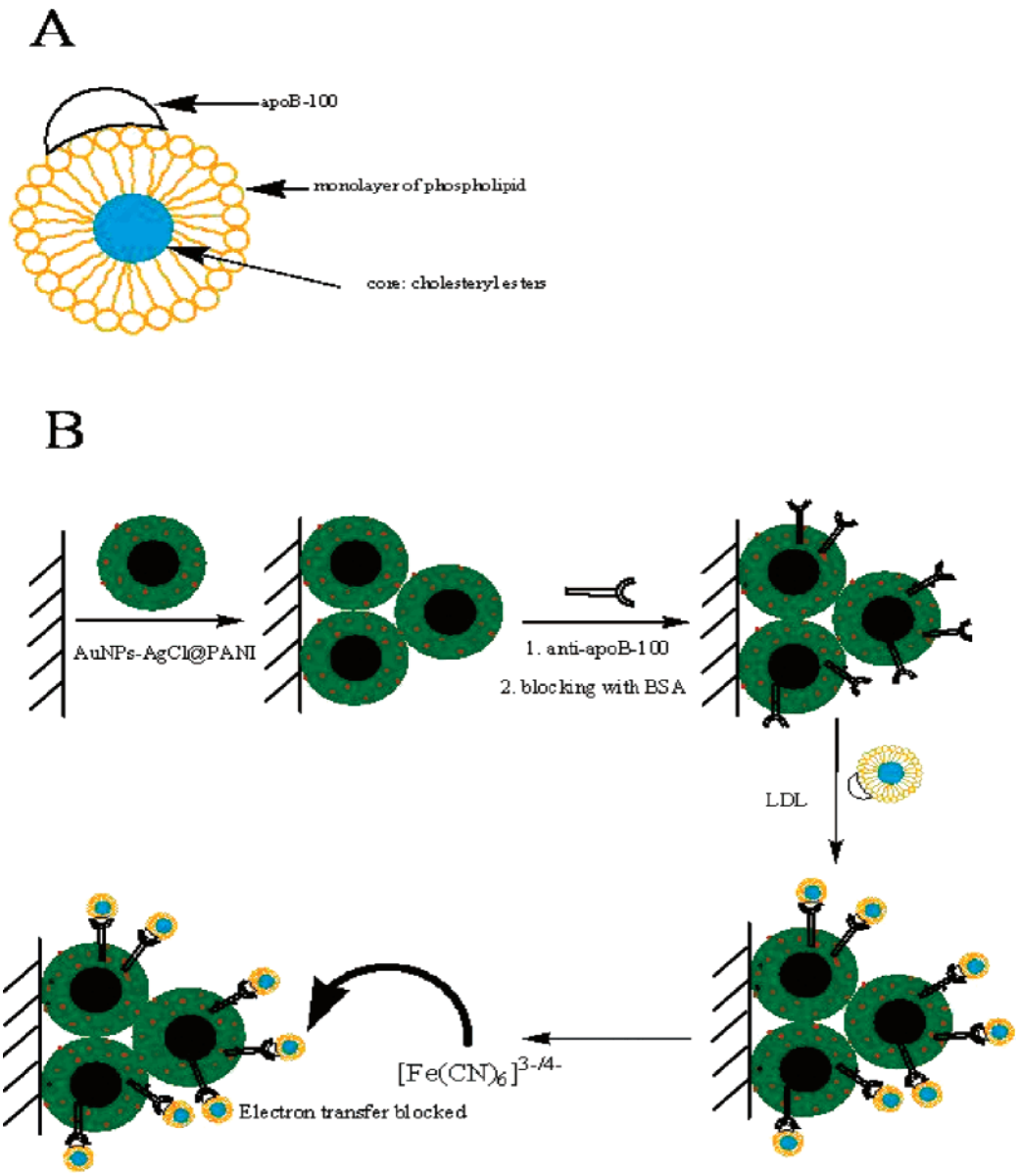

Figure 1. Structure of LDL (A). Schematic illustration of the process of fabrication of a LDL biosensor and the biosensing principle (B).

2. Experimental Section

2.1. Chemicals and Biochemicals. Silver nitrate, aniline, polyvinylpyrrolidone (PVP), hydrochloride (HCl), ammonium persulfate ($(NH_4)_2S_2O_8$, APS), and $HAuCl_4 \cdot 4H_2O$ were purchased from Shanghai Chemical Reagent Co. Aniline was distilled under reduced pressure. Bovine serum albumin (BSA) was obtained from Sigma Chemical Co. Anti-apoB-100 solution and plasma containing LDL of 6.7 mg/mL were provided by Nanjing Huibiao Biological Technology Co. and used as received. The $K_4[Fe(CN)]_6/K_3[Fe(CN)]_6$ mixture solution (1:1, 2 mM) used in EIS was prepared by 0.1 M phosphate buffer solution (PBS) of pH 7.0. All other reagents were of analytical grade and used without further purification, and distilled water was used throughout.

2.2. Preparation of AuNPs−AgCl@PANI Material and Fabrication of LDL Electrochemical Biosensor. AgCl@PANI nanocomposites were synthesized according to ref 11. $AgNO_3$ (0.012 M) and aniline (0.012 M) were added to 5% PVP aqueous solution. 5 mL of 1 M HCl aqueous solution of APS as oxidant was dropped into the above mixture under stirring. The reaction was allowed to proceed for 24 h.

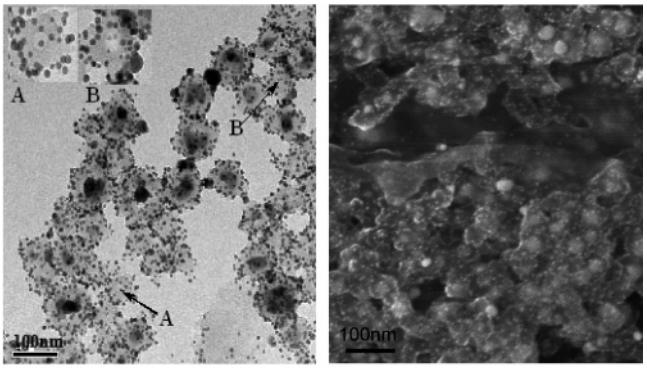

Figure 2. TEM (a) and SEM (b) of AuNPs−AgCl@PANI. The insets in (a) show the enlarged view of the regions arrows A and B pointed.

The Au colloid was prepared according to the reported method with some modifications by using KBH_4 as reductant and stabilized with sodium citrate.[21] 5 mL of 1% $HAuCl_4$ and 10 mL of 0.03 M sodium citrate were added to 250 mL of purified water and stirred. Then 5 mL of freshly prepared 0.1 M KBH_4 was added, and the solution color changed from

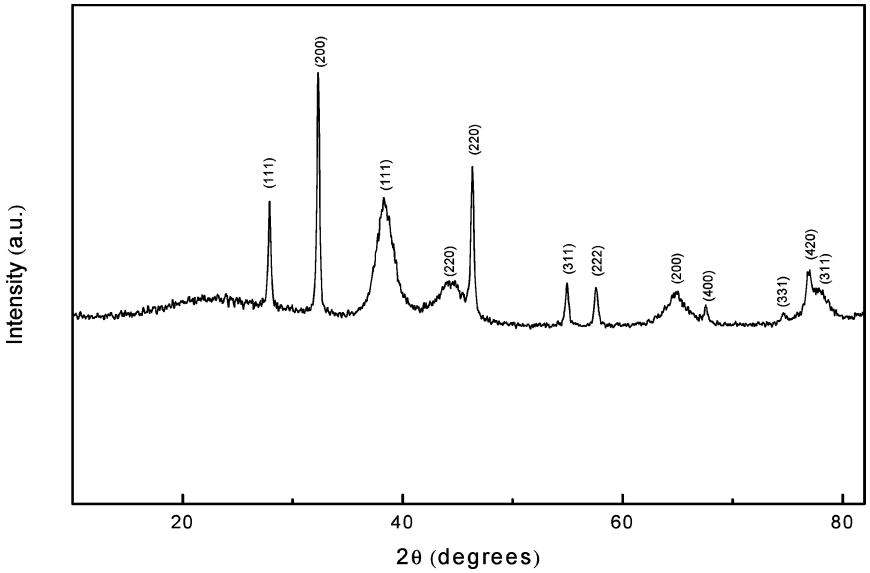

Figure 3. XRD patterns of AuNPs−AgCl@PANI.

colorless to wine red. Stirring was stopped, and the solution was left undisturbed for 2 h. The average diameter of the obtained AuNPs was about 5 nm.

30 mL of AgCl@PANI nanocomposites solution was added into 100 mL of Au colloid solution under stirring. The reaction was allowed to proceed for 12 h, and the resultant product was centrifuged and dispersed in water. AuNPs could be incorporated on the surface of AgCl@PANI nanocomposites, leading to the formation of AuNPs−AgCl@PANI hybrid material.

A GC electrode was polished to a mirror surface before each experiment with 0.05 μm α-Al_2O_3 slurry and then sonicated in distilled water and acetone successively. The cleaned electrode was dried with a stream of nitrogen immediately before use. The pretreated GC electrode was cast with 8 μL of the brown aqueous suspension of AuNPs−AgCl@PANI and then dried in air.

The prepared AuNPs−AgCl@PANI-modified GC electrode was incubated into the anti-apoB-100 solution overnight at 4 °C. After rinsing with PBS, the electrode was soaked in a 3% BSA solution at room temperature for 1 h to block active sites. Finally, the electrode was rinsed again with 10 mM PBS of pH 7.0 and stored at 4 °C when not in use.

The obtained LDL biosensor was incubated in 100 μL of 10 mM PBS (pH 7.0) solutions containing different LDL concentration at 37 °C for 50 min. After the specific antibody−antigen binding process, the immunosensor was rinsed with PBS and ready for impedance measurements. Figure 1B shows the schematic illustration of the biosensor construction process and the biosensing principle.

2.3. Apparatus. Electrochemical experiments were carried out at room temperature on a CHI660B electrochemical workstation (Chenhua, Shanghai, China) in a three-electrode configuration. A GC electrode (3 mm diameter) was used as a working electrode. A saturated calomel electrode (SCE) and a platinum electrode served as reference and counter electrode, respectively. All potentials given below were relative to the SCE. EIS was carried out in a buffered medium (0.1 M PBS, pH 7.4) containing 2 mM $K_4[Fe(CN)_6]/K_3[Fe(CN)_6]$ (1:1) mixture as the redox probe. The frequency was scanned from 100 kHz to 0.1 Hz at an open-circuit voltage of 0.15 V, acquiring 5 points/decade. The amplitude of sine voltage of 5 mV was used. The impedance Z is expressed in terms of a real (Z') and an imaginary ($-Z''$) component (Nyquist plot).

The morphology of AuNPs−AgCl@PANI was observed by transmission electron microscopy (TEM, JEM-1230) and scanning electron microscopy (SEM, LEO1530VP). X-ray diffraction patterns were taken on a Philip-X'Pert X-ray diffractometer with a Cu Kα X-ray source. All the attenuated total reflection Fourier transform infrared spectroscopic (ATR-FTIR) measurements were performed on a Bruker model VECTOR22. X-ray photoelectron spectroscopic (XPS) analysis was carried out on an ESCALAB MK II X-ray photoelectron spectrometer. The amount of Au within the composite was determined by thermogravimetric analysis (TGA) on a Shimadzu TGA-50 instrument from room temperature to 1200 °C at a heating rate of 10 °C /min in an air atmosphere.

3. Results and Discussion

3.1. Structure of AuNPs−AgCl@PANI Hybrid Material. The structure of AuNPs−AgCl@PANI can be confirmed directly by TEM and SEM images, as shown in Figure 2. The thickness of the PANI shell is about 20 nm, and the inside spots with about 25 nm diameter corresponding to the AgCl cores. The outside particles like gingili are AuNPs, showing that they have been modified onto the PANI surface. Some hollow AuNPs−AgCl@PANI, however, can also be observed, as shown in Figure 2a, and holes can be found on the PANI shell of these hollow AuNPs−AgCl@PANI (insets). The observation indicates that the AgCl cores have penetrated the PANI shell, leading to the formation of hollow AuNPs−AgCl@PANI.

Figure 3 illustrates the powder X-ray diffraction (XRD) patterns of AuNPs−AgCl@PANI material. As shown, the broad band appearing at a 2θ value of 25° is ascribed to the periodicity parallel to the polymer chains of PANI.[22] Another eight diffraction peaks (2θ = 27.9°, 32.3°,46.3°, 54.9°, 57.6°, 67.5° 74.6°, and 77.8°) correspond to Bragg's reflections from (111), (200), (220), (311), (222), (400), (331), and (420) planes of AgCl and are in good agreement with the reported data (JCPDS File No. 06-0480), showing the existence of AgCl nanoparticles in AuNPs−AgCl@PANI. Crystallite size of AgCl nanoparticles were calculated from the AgCl (111) diffraction line using Scherrer's equation, $L = k\lambda/\beta \cos \theta$, where L is the mean dimension of the crystallites, β is the full width at half-maximum of the diffraction peak, θ is the diffraction angle, λ is the wavelength of the Cu Kα radiation (0.1540 nm), and K is equal

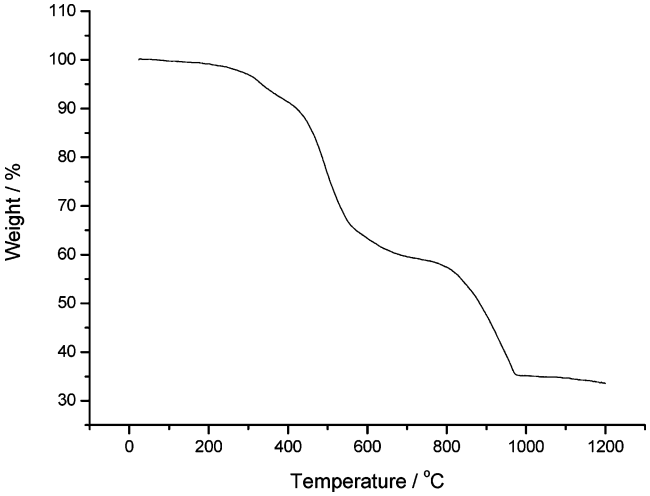

Figure 4. TGA curves for AuNPs−AgCl@PANI hybrid material.

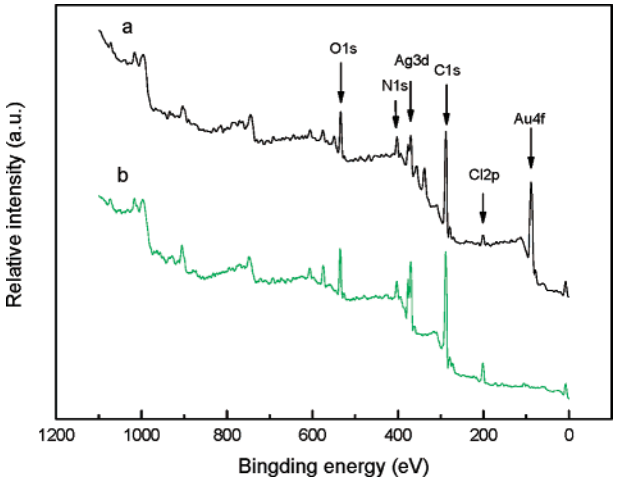

Figure 5. XPS of AuNPs−AgCl@PANI hybrid material (a) and AgCl@PANI nanocomposite (b).

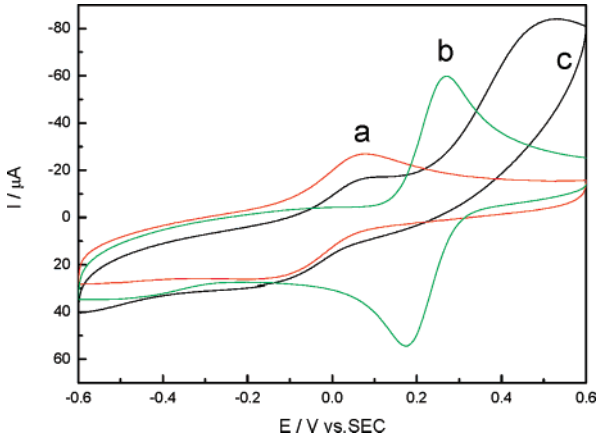

Figure 6. Cyclic voltammogram of AuNPs−AgCl@PANI-modified GC electrode in 0.1 M PBS (pH 7.0) (a) and cyclic voltammograms of bare GC electrode (b) and AuNPs−AgCl@PANI-modified GC electrode (c) in 0.1 M PBS (pH 7.0) containing 2 mM $[Fe(CN)_6]^{3-/4-}$.

to 0.89.[23] The calculated average size of AgCl is about 25 nm, which is consistent with the result from TEM and SEM (Figure 2). Four additional peaks at 38.3°, 44.2°, 64.8°, and 77.8° representing Bragg reflections from (111), (200), (220), and (311) planes of Au are observed,[24] and the crystallite sizes of Au nanoparticles could also be obtained using Scherrer's equation from the Au (111) diffraction line. The calculated average size of AuNPs in AuNPs−AgCl@PANI is about 5 nm, consistent with the result from Figure 2.

The AuNPs−AgCl@PANI material was also characterized by the thermogravimetric studies. Figure 4 illustrates the result of the thermogravimetric study on AuNPs−AgCl@PANI. Since Au does not qualify as a loss under the experimental conditions, the residual weight percentage (wt %) can be referenced to the content of Au in the hybrid material. The TGA curve shows a three-step weight loss. The weight loss in the first step at around 300 °C is attributed to the polymer degradation,[25] and the second weight loss step is attributed to the decomposition of PANI and PVP chains and the departure of residual acid dopant.[23] The third step, starting at around 800 °C, is due to the decomposition of AgCl. The total weight loss of AgCl@PANI is 65% under the experimental conditions. The residual weight percentage of AuNPs−AgCl@PANI is about 35%.

XPS was used to characterize the AuNPs−AgCl@PANI hybrid material (curve a) and the AgCl@PANI nanocomposites (curve b) in a wide scan. A new peak at 83.35 eV can be observed found for the AuNPs−AgCl@PANI material. The peak position corresponds to Au 4f, indicating the existence of Au NPs.[26] ATR-FTIR spectra could also be applied to characterize the AgCl@PANI and the AuNPs−AgCl@PANI materials. The peak corresponding to C═N stretching mode in AgCl@PANI appears at 1214 cm^{-1},[27] while AuNPs−AgCl@PANI has it at 1243 cm^{-1}, indicating that AuNPs do not adsorb on AgCl@PANI nanocomposites through electrostatic interaction because the PANI shell has been doped by large amounts of negative charges. The quinoid nitrogen atoms have offered their lone-pair electrons to the empty orbits of AuNPs, and coordination bonds are formed between nitrogen atoms and AuNPs.

The cyclic voltammogram obtained at AuNPs−AgCl@PANI-modified GC electrode in 0.1 M PBS (pH 7.0) is shown in Figure 6 (curve a). AuNPs−AgCl@PANI showed good electrochemical behavior at neutral pH environment. Generally, PANI is redoxactive only in acid media (pH < 4), which has restricted its applications in bioelectrochemistry. However, it was reported that doping PANI with negatively charged sulfonate units,[28] or the incorporation of negatively charged poly(acrylic acid)[29] or DNA units,[30] yielded a redox-active polymer at neutral and even basic aqueous solution, and we believe that negatively charged groups associated with the AgCl cores have provided anionic doping. Moreover, AuNPs stabilized with sodium citrate could offer additional negative charges, resulting in the excellent electroactivity of AuNPs−AgCl@PANI in neutral aqueous solution. Cyclic voltammograms obtained at bare GC electrode (curve b) and AuNPs−AgCl@PANI-modified GC electrode (curve c) in 0.1 M PBS (pH 7.0) containing 2 mM $[Fe(CN)_6]^{3-/4-}$ are also shown in Figure 6. Because of the plenty negative charges carried by citrate-stabilized AuNPs, the cathodic peak current of ferricyanide could hardly be observed at the AuNPs−AgCl@PANI-modified GC electrode, suggesting that the electron transfer between $[Fe(CN)_6]^{3-/4-}$ and GC electrode has been blocked severely. The anodic peak current of ferricyanide, however, increased greatly (curve c). It has been widely accepted that nanoscaled gold particles have some important size-dependent properties due to the quantum size effect. The surface of metallic nanoparticles is always electron-deficient, and the affinity to electrons will increase with the decrease of dimension.[31] As the diameter of the AuNPs in the hybrid material is about 5 nm, the AuNPs can act as strong electron acceptors to adsorb electrons from $[Fe(CN)_6]^{4-}$; thus, oxidation of ferricyanide was catalyzed, leading to the increase of anodic peak current.

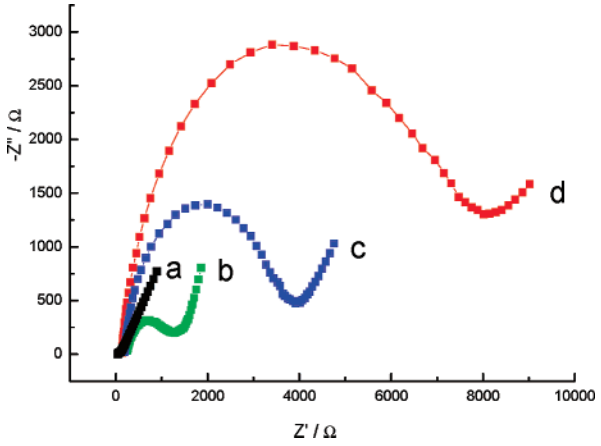

Figure 7. Nyquist diagram ($-Z''$ vs Z') for Faradaic impedance spectra in PBS (pH 7.0) containing 2 mM $[Fe(CN)_6]^{3-/4-}$ for a bare GC electrode (a), after modified with AuNPs−AgCl@PANI (b), after adsorption of anti-apoB-100 (c), and after saturation with BSA (d).

The LDL biosensor was fabricated by adsorbing anti-apoB-100 on an AuNPs−AgCl@PANI modified GC electrode. The free active sites of the biosensor were blocked with BSA, and EIS was performed in the presence of the redox probe $[Fe(CN)_6]^{3-/4-}$ at the scanning frequency from 0.1 to 100 000 Hz to characterize each step of the construction process of LDL biosensor (Figure 7). The impedance spectrum includes a semicircle portion corresponding to the electron-transfer-limiting process and a linear part resulting from the diffusion-limiting step of the electrochemical process.[16] The diameter of the semicircle exhibits the electron-transfer resistance (R_{et}) of the layer, which controls the electron-transfer kinetics of the redox probe at the electrode interface. Thus, the diameter can be used to describe the interface properties of the electrode.[15] It can be seen in Figure 7 that R_{et} of bare GC electrode increased greatly after deposition of AuNPs−AgCl@PANI (curves a and b), which is consistent with the result of Figure 6. Since the insulating property of proteins, immobilization of antibody on the electrode surface generated the insulating protein layer, resulting in additional increase in R_{et} (curve c). After saturation of the free active sites of the electrode with BSA, the electron transfer of $[Fe(CN)_6]^{3-/4-}$ was blocked further due to the insulation of BSA (curve d). BSA had played a very important role in the construction of LDL biosensor. In control experiments, LDL was found to be able to be nonspecifically adsorbed on the surface of AuNPs−AgCl@PANI, and BSA could prevent LDL from nonspecific adsorption.

The prepared biosensor was rinsed with PBS and then incubated in solutions containing different concentration of LDL. The LDL in solution could be bonded to the electrode surface through the specific antigen−antibody reaction between apoB-100 and anti-apoB-100, which could be reflected by the differences in R_{et} values (ΔR_{et}) of the immunosensor between the before and after incubation with LDL. The effects of incubation temperature and incubation time on the immunoreaction were studied. Figure 8A depicts the relationship of ΔR_{et} with incubation time. It can be seen that ΔR_{et} increased first with the increase of reaction time and then reached a plateau after 50 min. The relationship of ΔR_{et} with incubation temperature is shown in Figure 8B, and the maximum of ΔR_{et} could be observed when it was at 37 °C. Thus, 50 min of incubation time and 37 °C as incubation temperature were selected for the immunoassay of LDL.

Before impedance measurements were performed, cyclic voltammetry (CV) was carried out until the currents did not

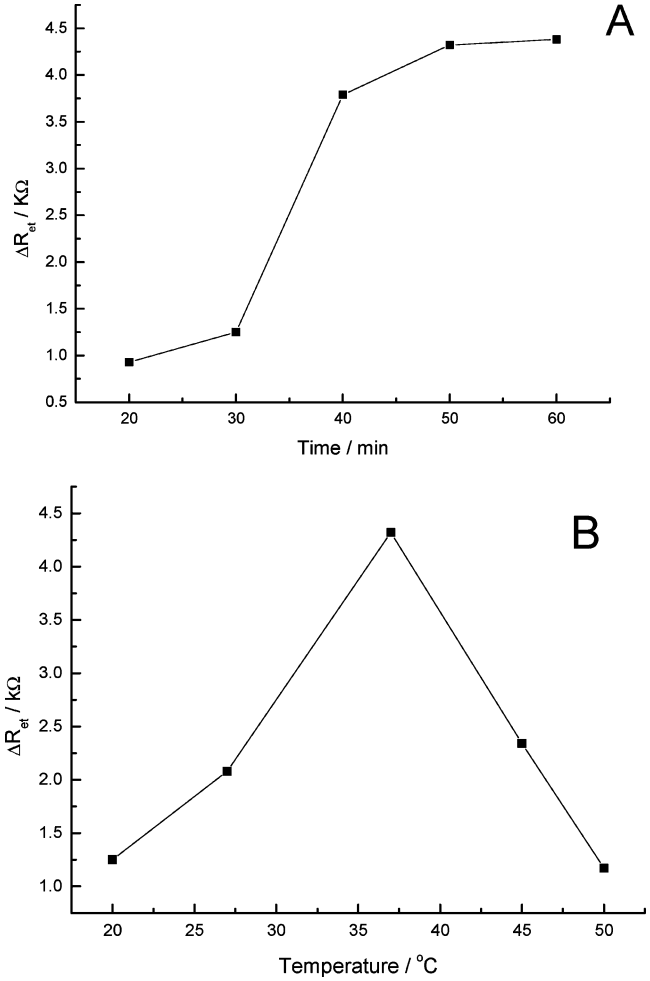

Figure 8. Relationships of ΔR_{et} with the incubation time (A) and incubation temperature (B). Faradaic impedance spectra were obtained in PBS (pH 7.0) containing 2 mM $[Fe(CN)_6]^{3-/4-}$.

change anymore. For each measurement, because EIS was performed when the diffusion layer had grown sufficiently, the biosensor showed good reproducibility. The relative standard deviation (RSD) of five successive measurements to 1.34 pg/mL of LDL was 1.9%. Figure 9A shows the impedance spectra obtained in 2.0 mM $[Fe(CN)_6]^{3-/4-}$ solution (pH 7.0) after incubation with different concentration of LDL. It can be seen that R_{et} increased with the increase of LDL concentration, and Figure 9B illustrates a linear relationship of ΔR_{et} with the logarithm of the concentration of LDL in a range from 0.34 to 13.4 pg/mL ($r = 0.994$, $n = 6$).

The structure of LDL contains a hydrophobic core cholesteryl ester surrounded by coat of phospholipids. The isoelectric point of LDL is 5.4, and LDL is negatively charged when pH value is 7.0.[32] The electron transfer of $[Fe(CN)_6]^{3-/4-}$ redox couple will be blocked severely due to the plenty of negative charges carried by the phospholipids coat of LDL. In addition, the LDL conductivity was very poor;[6] thus, small amounts of LDL on the electrode surface could result in great changes in R_{et}. Since the high surface-to-volume ratio of AuNPs−AgCl@PANI, which could provide surface for high enzyme loading, the sensor showed a extremely sensitive response to LDL with a detection limit of 0.34 pg/mL.

Nonspecific interaction tests between the immunosensor and other proteins (such as hIgG and CRP) were performed. Nonspecific adsorption is the major problem in label-free immunosensing.[17] Both the dectected ΔR_{et} caused by 100 pg/

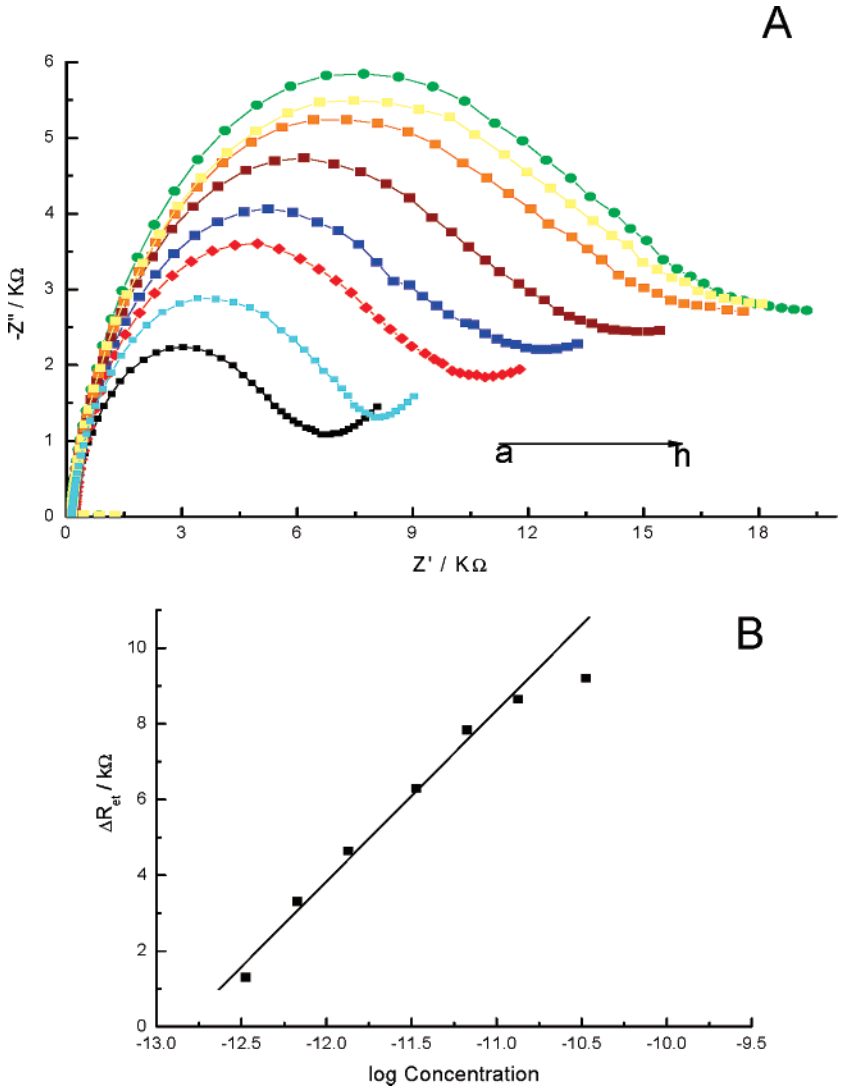

Figure 9. Nyquist diagram ($-Z''$ vs Z') of Faradaic impedance spectra in PBS (pH 7.0) containing 2 mM $[Fe(CN)_6]^{3-/4-}$ for the immunosensor after incubation with solutions containing different concentration of LDL: (a) 0, (b) 0.34, (c) 0. 67, (d) 1.34, (e) 3.35, (f) 6.7, (g) 13.4, and (h) 33.5 pg/mL (A). Relationship of ΔR_{et} with the logarithm of LDL concentration (B).

mL proteins were neglectable compared with the response of the biosensor (2.3 KΩ) to 0.34 pg/mL of LDL.

4. Conclusion

The AuNPs−AgCl@PANI core−shell nanocomposites have used to fabricate a novel biosensor. A sensitive label-free LDL electrochemical biosensor was constructed by immobilizing anti-apoB-100 on an AuNPs−AgCl@PANI-modified GC electrode. The large specific surface area of the hybrid material could provide surface for high antibody loading. As the poor conductivity of LDL as well as the negative charges carried by LDL phospholipids coat, the biosensor exhibit highly sensitive response to LDL with a detection limit of 0.34 pg/mL. The AuNPs−AgCl@PANI hybrid material can provide a new electrochemical platform for designing bioelectrochemical sensors of high sensitivity.

Acknowledgment. We greatly appreciate the support of the National Natural Science Foundation of China for Distinguished Young Scholars (20325516), the Key Program (20635020), Creative Research Group (20521503). This work is also supported by National Basic Research Program of China (2006CB933201). The authors thank the European Commission Sixth Framework Program through a STREP grant to the SELECTNANO Consortium, Contract No. 516922, for financial support.

References and Notes

(1) Cheng, T. O. *Chin. Med. J.* **2005**, *118*, 355−359.
(2) Lusis, A. J. *Nature (London)* **2000**, *407*, 233−241.
(3) Couto, R. D.; Dallan, L. A. O.; Lisboa, L. A. F.; Mesquita, C. H.; Vinagre, C. G. C; Maranhao, R. C. *Lipids* **2007**, *42*, 411−418.
(4) Orlova, E. V.; Sherman, M. B.; Chiu, W.; Mowri, H.; Smith, L. C.; Gotto, A. M. *Proc. Natl. Acad. Sci. U.S.A.* **1999**, *96*, 8422−8429.
(5) Hevonoja, T.; Pentikainen, M. O.; Hyvonen, P.; Kovanen, P. T.; Ala-Korpela, M. *Biochim. Biophys. Acta* **2000**, *1488*, 189−210.
(6) Clauss, S. B.; Kwiterovich, P. *Progr. Pediatr. Cardiol.* **2003**, *17*, 123−130.
(7) Nassar, B. A.; Dunn, J.; Title, L. M.; O'nell, B. J.; Kirkland, S. A.; Zayed, E.; Bata, I. R.; Cantrill, R. C.; Johnstone, J.; Dempsey, G. I.; Tan, M.-H.; Breckenridge, W. C.; Johnstone, D. E. *Clin. Biochem.* **1999**, *32*, 275−282.
(8) Fei, H.; Maeda, S.; Kirii, H.; Fujigaki, S.; Maekawa, N.; Fujii, H.; Wada, H.; Saito, K.; Seishima, M. *Clin. Chem.* **2000**, *46*, 1351−1356.
(9) Liu, K.-Z.; Shi, M.; Man A.; Dembinski, T. C.; Shaw, R. A. *Vib. Spectrosc.* **2005**, *38*, 203−208.
(10) Snellings, S.; Fuller, J.; Pitner, M.; Paul, D. W. *Biosens. Bioelectron.* **2003**, *19*, 353−363.
(11) Feng, X.; Liu, Y.; Lu, C.; Hou, W.; Zhu, J.-J. *Nanotechnology* **2006**, *17*, 3578−3583.
(12) Gangpadhyay, R.; De, A. *Chem. Mater.* **2000**, *12*, 608−622.

(13) Tian, S. J.; Liu, J. Y.; Zhu, T.; Knoll, W. *Chem. Mater.* **2004**, *16*, 4103−4108.
(14) Diaz, A. F.; Logan, J. A. *J. Electroanal. Chem.* **1980**, *111*, 111−114.
(15) Hleli, S.; Martelet, C.; Abdelghani, A.; Bessueille, F.; Errachid, A.; Samitier, J.; Hays, H. C. W.; Millner, P. A.; Burais, N.; Jaffrezic-Renault, N. *Mater. Sci. Eng., C* **2006**, *26*, 322−327.
(16) Chen, H.; Jiang, J.-J.; Huang, Y.; Deng, T.; Li, J.-S.; Shen, G.-L.; Yu, R.-Q. *Sens. Acutators B* **2006**, 117, 211−218.
(17) Zhang, S.; Huang, F.; Liu, B.; Ding, J.; Xu, X.; Kong, J. *Talanta* **2007**, *71*, 874−881.
(18) Bart, M.; Stigter, E. C. A.; Stapert, H. R.; Jong, G. J. D. Bennekom, W. P. V. *Biosens. Bioelectron.* **2005**, *21*, 49−59.
(19) Rahman, M. A.; Shiddiky, M. J. A.; Park, J.-S.; Shim, Y.-B. *Biosens. Bioelectron.* **2007**, *22*, 2464−2470.
(20) Darin, F.; Park, D.-S.; Park, J.-S.; Shim, Y.-B. *Biosens. Bioelectron.* **2004**, *19*, 1245−1252.
(21) Zhou, N.; Wang, J.; Chen, T.; Yu, Z.; Li, G. *Anal. Chem.* **2006**, *78*, 5227−5230.
(22) Pillalamarri, S. K.; Blum, F. D.; Tokuhiro, S. T.; Story, J. G.; Bertino, M. F. *Chem. Mater.* **2007**, *17*, 227−229.
(23) Gao, Y.; Jiang, P.; Liu, D. F.; Yuan, H. J.; Yan, X. Q.; Zhou, Z. P.; Wang, J. X.; Song, L.; Liu, L. F. Zhou, W. Y.; Wang, G.; Wang, C. Y.; Xie, S. S. *J. Phys. Chem. B* **2004**, *108*, 12877−12881.
(24) Tsai, C. Y.; Lee, D. S.; Tsai, Y. H.; Chan, B.; Luh, T. Y.; Chen, P. J.; Chen, P. H. *Mater. Lett.* **2004**, *58*, 2023−2026.
(25) Wei, Y.; Hsueh, K. F. *J. Polym. Sci., Part A: Polym. Chem.* **1989**, *27*, 4351−4363.
(26) Feng, X.; Mao, C.; Yang, G.; Hou, W.; Zhu, J.-J. *Langmuir* **2006**, *22*, 4384−4389.
(27) McCarthy, P. A.; Huang, J.; Yang, S. C.; Wang, H. L. *Langmuir* **2002**, *18*, 259−263.
(28) Bartlett, P. N.; Wang, J. H. *J. Chem. Soc., Faraday Trans.* **1996**, *92*, 4137−4143.
(29) Bartlett, P. N.; Simon, E. *Phys. Chem. Chem. Phys.* **2000**, *2*, 2599−2606.
(30) Xiao, Y.; Kharitonov, A. B.; Patolsky, F.; Weizmann, Y.; Willner, I. *Chem. Commun.* **2003**, *13*, 1540−1541.
(31) Henglein, A.; Mulvaney, P.; Linnert, T. *J. Chem. Soc., Faraday Discuss.* **1991**, *92*, 31−44.
(32) Sonmez, H.; Ozturk, Z. G.; Ulutin, T.; Domanic, N.; Glu, E. K. *Thrombosis Res.* **2000**, *99*, 311−315.